Int J Adv Manuf Technol (2017) 88:127–145
DOI 10.1007/s00170-016-8707-0

ORIGINAL ARTICLE

Welding seam profiling techniques based on active vision sensing for intelligent robotic welding

Jawad Muhammad[1] · **Halis Altun**[2] · **Essam Abo-Serie**[1]

Received: 29 November 2015 / Accepted: 31 March 2016 / Published online: 21 April 2016

Abstract Intelligent robotic welding involves replicating the role of a manual professional welder to adaptively control the welding process. This is necessary to achieve accurate, fast and high-quality welding process in addition to the challenging factors for humans to operate in the welding environment. Therefore, robotic welding exists since the early days of robotics and it is still an active research area. This is why there have been numerous researches in this area for a very long time. Among various techniques proposed by researchers for the adaptive control of the robotic welding process, vision-based control is the most popular due to its non-invasiveness. Therefore, in this paper, we review, analyse and categorise the proposed vision-based techniques with the aim of covering the different image processing and feature extraction aspect of the techniques. The focus is mainly on the active vision system where various image processing techniques have been utilised in extracting the welding seam features. The challenges and difficulties to extract seam features in active vision system have been highlighted. The trends and new approaches have been indicated in order to provide a comprehensive source for researchers who are planning to carry out research related to the intelligent robot vision techniques for welding automation.

Keywords Survey on active vision · Survey on seam finding · Survey on intelligent robotic welding · Survey on seam tracking · Robotic arc welding · Robotic laser welding · Welding automation · Laser vision sensor · Machine vision · Feature extraction

✉ Jawad Muhammad
jmuhammad@mevlana.edu.tr

[1] Mevlana Universitesi, Konya, Konya, Turkey

[2] Karatay University, Konya, Konya, Turkey

1 Introduction

Robotic welding is one of the oldest and most rapidly growing areas for robotics applications. However, fully automated robotic welding system is yet to be effectively achieved. This is due to the harsh environmental conditions created by the welding process and various factors such as welding spatter and arc lights disturbance, vigorous welding structure types, distortions due to welding heat generation and varying structure of the welding seams [1]. These factors collectively affect the realisation of a fully automated robotic welding system. Intelligent robotic welding system comprises three basic components as shown in Fig. 1: (1) tracking and profiling of welding seam and pool, (2) robot trajectory planning and control [2–8] and (3) welding process parameter control [9–12]. Tracking and profiling of welding seam provide information for robot trajectory planning and control. It is also a crucial step in controlling welding parameters to match the requirements set for achieving high-quality welding. As there are plenty of different research directions on the tracking and profiling of welding seam and pool, in this review, we will focus on describing and categorizing the proposed approaches in this field. The aim is to give a comprehensive insight by exploring the available techniques proposed in the literature and by indicating the cons and pros of the techniques. The review will only be limited to the first component of welding system (tracking and profiling of welding seam); the second and third components will not be covered in this review.

Methods in tracking and profiling welding pool and seam can be categorised into (i) vision-based sensing and (ii) non-vision-based sensing methods. The most common non-vision-based sensing method is the *through-arc sensing* method. The method uses the electrical parameters from the welding arc and the knowledge about the motion of the weld torch which is controlled by the welding robot [1, 9, 13]. The through-arc

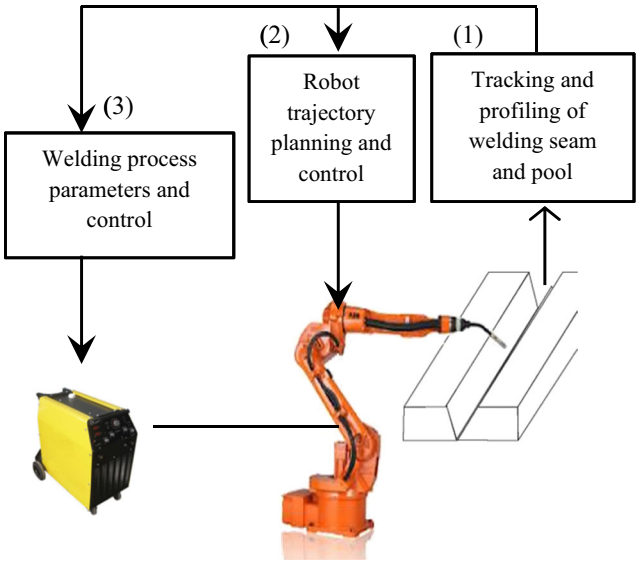

Fig. 1 Intelligent robotic welding components

sensing method involves the use of the change in the current when the distance between the contact tube and the workpiece varies [1]. This is considered one of the oldest methods for seam tracking and profiling. Although it is relatively easy and cost-effective to use, it is generally considered as less accurate than the optical sensing methods and cannot be used to profile a complex seams and molten welding pool during welding [1]. Research on finding geometrical properties of both seam and pool using optical sensing method can be further categorised based on either *passive vision* or *active vision* methods. The distinction between these two methods relies on the use of the optional light source. In the active vision, a camera device and a light source are used while in the *passive* vision, two camera devices are used without a light source. The image processing algorithms used in either of these methods significantly differ as the active vision system becomes much easier than the former due to the simplicity of using an external light source to mark and profile the welding workpiece.

Using the passive vision system, two sets of information can be obtained: (1) the seam profile which can alternatively be acquired using active vision and (2) the welding pool profile which can only be acquired with passive vision. More so, passive vision systems can be used to acquire the seam path holistically as opposed to active vision which only provides one point at a time. Numerous techniques have been proposed for the image pre-processing, seam profiling and weld pool profiling of the passive vision system. For the pre-processing, filtering the image with combination of filters such as Gaussian filter [14, 15], median filter [14, 16–19], Laplacian [16] filter, etc. to suppress high-frequency noise such as the strong welding arc light is popular among many authors [14, 15]. For the welding seam profiling, various methods are proposed such as grey-level distribution methods [14, 16, 18, 20] that consider the darkness characteristic of the welding seam region, conventional edge detection methods like Canny edge detection [15, 21–24] and Sobel edge detection [19, 25] that extract edges in the image from which the seam is then extracted and template matching method [17, 26, 27] that searches for a known pattern in an image using a predefined template which identifies the seam. Some authors proposed method of detecting the seam edges at sub-pixel accuracy [28]. For the welding pool profiling, the basic task is detecting the edges of the welding pool from which the pool dimensional features can be determined. Various methods have been proposed by researchers to detect the pool edges, among which is the use of conventional edge detection methods [29–31] such as Canny and Sobel edge detections. Another notable technique is the histogram analysis methods [32–35] that analyse the histogram of the welding pool image in order to obtain the boundaries of the pool as the edges. Grey-level processing methods [36–42] are also another proposed method that detects the edges by directly evaluating the pixel grey values and its neighbourhood. In [38, 39, 42], unlike the traditional weld pool profiling that considers only the outer edges of the pool, the grey values of the whole region of the welding pool are analysed and the centroid position is calculated as a function of the gradient distribution of the whole weld pool image. In [9], the grey-level jumps (abrupt change in grey-level values) which correspond to the edge boundaries of the pool are determined. A search is performed from the centre of the image to its exterior, and the pixels with grey-level jumps are detected as the edge pixels.

In this review, the main focus will be on the active vision system techniques for extracting the seam geometrical information. The system improvements using different image processing and pattern recognition algorithms will be discussed in detail. In the subsequent sections, the contributions in the literature made by various authors in the active vision methods will be presented. The presentation only considers the methodology adopted or developed by different authors as there is no any avenue to compare or evaluate the effectiveness of their proposed methods. This is attributed to the fact that a fair comparison on the accuracy and performance of the available methods does not only depend on the image processing and pattern recognition algorithms, but also depend on other factors such as welding environment condition, workpiece type used, image sensor type, camera resolution, calibration parameters, etc. The recent approaches to overcome these challenges of improving the system accuracy will also be discussed.

2 Active vision systems

The principle of active vision system is primarily based on triangulation technique [43] as shown in Fig. 2. An active vision system comprises an image sensor (camera device), an external light source and optical lenses and filters. It simply

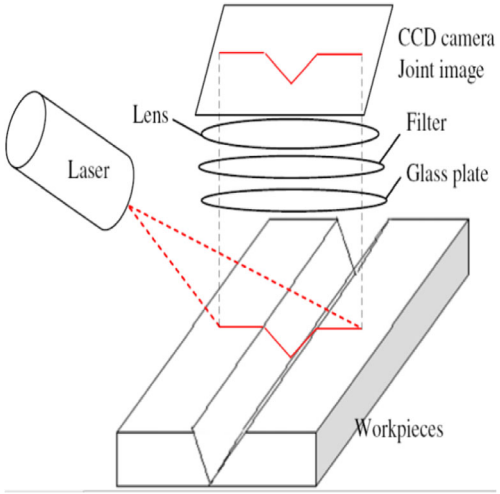

Fig. 2 Active laser vision system [43]

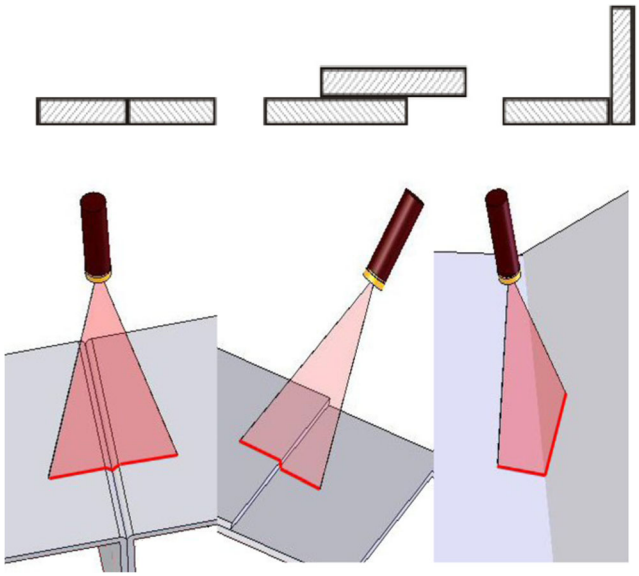

Fig. 3 Joint configurations from left to right, butt, overlap and corner joint and their corresponding laser deformations [21]

involves the projection of a structured light on the welding joint, capturing the pattern produced on the joint by the light using a camera device and processing the captured image to extract the geometrical information of the welding joint. The nature and pattern of the structured light captured by the camera depend on six factors [44, 45]:

- *The type of the welding joint configuration and preparation*: There are basically three types of welding joint configurations [44] (butt, overlap and corner joint) as shown in Fig. 3. A lot of other joint configurations could be formed by the combination of these three configurations. Each joint configuration has its own method of preparation before a welding is performed as shown in Fig. 3.
- *Pattern of the structural laser light source*: Two forms of structured light source patterns can be used (line shape and 2D structured light shapes) as shown in Fig. 4. The use of different pattern of structured light depends on the geometrical information required to be extracted from the welding seam. Using a line laser stripe, the position information of the line of projection can be extracted as well as the rotation around the axis of projection [49–53]. In 2D shape structured light, all positions and also orientations are measurable along the plane of the 2D shape. Different 2D structural light patterns have been used by many authors: circle [46], multiple lines [48, 54, 55], triangle [44, 56], cross [47, 56], etc.
- *Optical properties of the welding part surfaces*: Optical properties of the welding part affect the quality of the reflected light due to various surfaces optical attributes. Highly translucent welding part surface with low reflective index can cause the laser light to be scattered into the welding joint, thereby appearing distorted to the camera; this produces an image pattern with a very low signal-noise ratio [45]. Likewise, a Lambertian surface material will cause more direct reflection on the surface, and consequently, the camera acquires higher signal-noise ratio image [45].
- *The location of the light relative to the torch*: The noise generated from the torch can make the light pattern invisible and difficult to detect. The torch location is considered as a source of light, and the light intensity decreases with square of the distance. It is therefore more challenging as seam recognition becomes closer to the torch.
- *Camera and laser quality*: One other major factor affecting the quality of the image is the camera and laser quality. Because of the high intensity of light produced from the welding, a camera of high dynamic range is usually recommended. The laser thickness also assists in receiving a thin beam or pattern and therefore improves the accuracy. However, these system requirements make the system more expensive. Successful image processing techniques can reduce that cost by relaxing the camera and laser specifications.

The image of the pattern captured by the camera, in practice, has some discontinuities and different widths along its length. These are caused by various surface reflectivities and possible metal spatter on the joint. Therefore, complex image processing and pattern recognition algorithms are necessary in order to effectively extract accurate geometrical information of the welding joint. The image processing and pattern recognition algorithms can be divided into three sequential subprocesses as follows:

- Image pre-processing
- Extraction or segmenting of the laser stripe pattern from the captured image

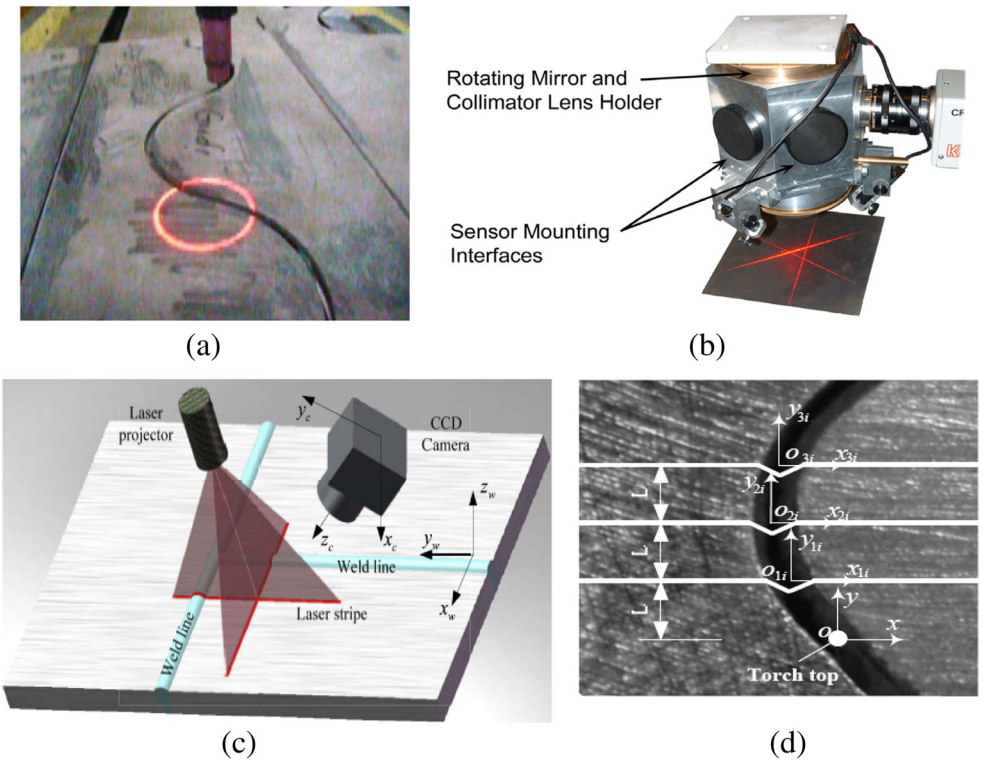

Fig. 4 Two-dimensional laser shapes: **a** circle [46], **b** triangle [44], **c** cross [47] and **d** multiple lines [48]

- Welding joint feature extraction and profiling

By examining the literature, it was found out that most authors contribute in these three sub-processes. A careful discussion of different publications which are sorted according to its relevance in each of these sub-processes will be carried out and presented in the following sub-sections.

2.1 Image pre-processing

Before image processing and pattern recognition process, a compulsory image enhancement and noise removal step are common practices. This is particularly important in robotic welding as it entails a lot of noise from the arc glares, welding smoke and spatters during the welding. Due to the nature of the noise in welding environment which is usually a salt-and-pepper natured noise, median filtration was proposed by authors [21, 43, 48, 49, 55, 57–60], to enhance the input image before performing any process on the input image. The main advantages of median filtering are that it is more efficient, and it has good performances in filtering white and long trail noises [59]. The median filter can also keep the detail information such as edge pieces and sharp angles of seam. In median filtering, the input intensity is replaced by the median of the intensities contained in its neighbourhood pixels. The size of the filter used depends on the welding application and the welding system configuration. Filtering the image with a Gaussian filter has also been adopted by many researchers [52, 58, 61]. Due to the fact that Gaussian filter suppresses high-frequency noise by smoothening the image, employing this filtering strategy with welding images is not so popular among researchers. However, some researchers claimed that the use of a Gaussian filter with a larger kernel size can enhance the image [52, 61]. A recent comparison study performed on the use of a median filter and Gaussian filter showed that median filter can give better enhancement effect [58]. Further filtration using a morphological filter has been employed to improve the image quality [55, 58]. After median filtering, an additional filtration was performed with erosion and dilation mask which help in supressing the noise [55]. A comparison study performed on the use of erosion, dilation, closing and opening filters after median filtering showed that the closing filter can provide better performance [58].

Due to the dynamics that is involved in industrial environment such as that of welding, use of conventional filters such as median and Gaussian filters has not been always the case among many researchers. Researchers have proposed various other techniques to filter out noise, among which is the multiple frame processing that uses images from consecutive sequence of frames to filter out noise [3–5, 51, 53, 62, 63]. The use of such filtering technique is attributed to the fact that the welding arc and splash spatter noise have the characteristics of instantaneity. In general, the noise in the welding environment lasts for less than one sample period, whereas the seam and laser stripe in the image are stable [63]. The operation involves taking the smallest intensity of the corresponding pixels in the

images. Sometimes, instead of taking the smallest intensity, differential frame can also be calculated by subtracting the grey values of all the corresponding pixels in the images as shown in Fig. 5 [51]. The differential frame is then thresholded and used as a mask to suppress noise in the original frame. Another approach of multiple frame processing for image enhancement is the background subtraction technique [64]. The concept is based on detecting the moving objects from the difference between the current frame and a reference frame often called the "background image" or "background model." However, due to the complex nature posed by the welding environment and dynamic nature of foreground and background noises, adopting a background model is almost impossible.

Another approach in noise removal for active vision is the utilisation of colour information. Since the red component which is commonly used to form the laser strip in an RGB-coloured image has the highest signal-noise ratio. Selecting the red plane instead of the traditional conversion of the three RGB channels to single channel (converting the image to grey) can enhance the laser stripe object in the image [47]. This approach could be challenging especially during the welding process whereby welding arc glare noise is usually white coloured of which, it is saturated in all the three planes of the RGB image. Hence, this signifies that the white arc together with red component will appear as a noise. However, instead of taking the red plane, the image can be converted into hue saturation value (HSV) colour space first and then thresholding the HSV channels to choose the red colour in the image.

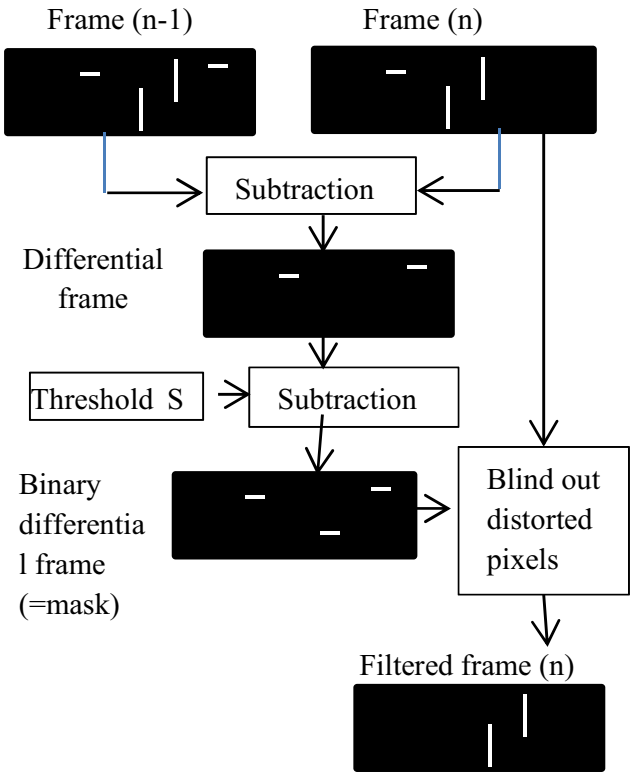

Fig. 5 Principle of binary differential method (BDM) to filter out distortions caused by spatter [51]

Some researchers [57, 58] proposed direct image thresholding to remove low-intensity noise in the image and convert the image into binary as an effective pre-processing step. Recursive use of Otsu thresholding algorithm [65] was employed to enhance the laser stripe pattern in the input image by converting the image into a binary image with less noise. At first, Otsu thresholding is applied to the input image to segment the input image into two regions. The region above the Otsu threshold is preserved, and the Otsu thresholding is applied again to the region below the Otsu threshold value. This iteration continues until a criteria ε given by (1) is reached [57].

$$\varepsilon = \frac{N_{(J-1)} - N_{(J)}}{N_{(J)}} - \frac{\sigma_{W(J-1)} - \sigma_{W(J)}}{\sigma_{W(J-1)}} \quad (1)$$

where $N_{(J-1)}$ and $N_{(J)}$ are the total pixel numbers of the previous and the present segmented image, respectively, $\sigma_{W(J-1)}$ and $\sigma_{W(J)}$ are the interclass variances of the previous and present segmented image. Figure 6 shows the result of segmentation using Otsu and the recursive improved Otsu thresholding proposed by [57] under various signal to noise ratios.

Based on the above discussions, it can be observed that among all these methods stated, the most popular pre-processing sequence adopted by majority of the authors is the step of applying a median filter to the original image. Although there is some studies where the Gaussian filtration is employed, it is perceived to be not suitable in this application as it will suppress the high-frequency component in the laser line image and cause the loss of information. However, some of the proposed algorithms may be used together to produce a more efficient hybrid pre-processing scheme. As the welding process is not a time critic application and the availability of high-computational power of today processors, the hybridisation of the proposed algorithm seems to be feasible. One of such hybrid algorithm can be achieved by combining the multiple frame processing [3–5, 51, 53, 62, 63] and the median filtration [21, 43, 48, 49, 55, 57–60]. Also, it is possible to improve the quality of image further by using a morphological filter as in [55, 58].

2.2 Extraction of laser stripe pattern

Extraction of the laser stripe pattern depends on the structure and shape of the pattern used. Extracting the pattern involves generation of a location vector that describes the position of the laser stripe pattern in an input image. Several methods are proposed in the literature. In this section, as far as the laser stripe extraction is concerned, a categorisation of methods that are reported in the literature will be listed, together with a

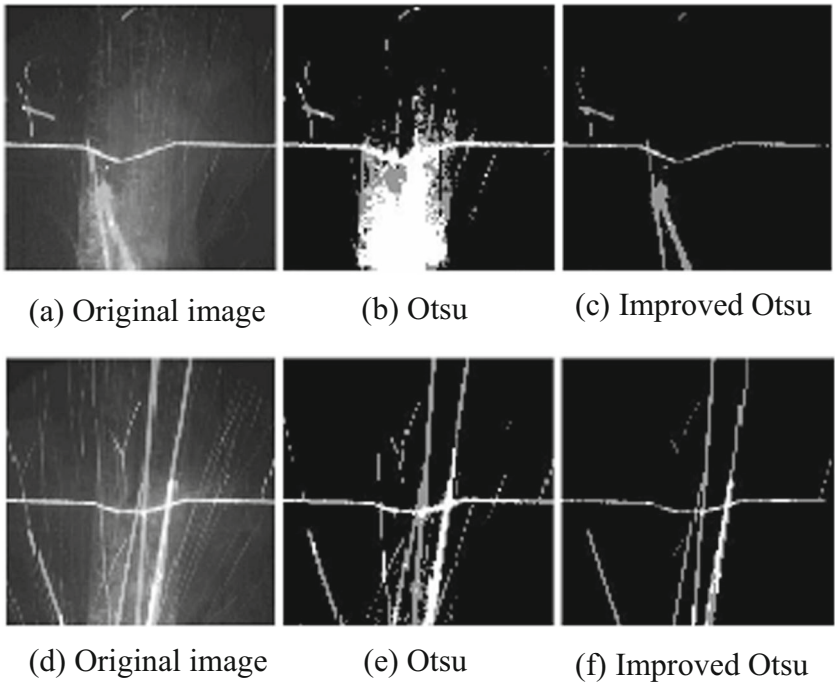

Fig. 6 **a**–**c** Segmentations of seam image with a noise to signal ratio of 13. **d**–**f** Segmentations of seam image with a noise to signal ratio of 18 [57]. **a** Original image. **b** Otsu. **c** Improved Otsu. **d** Original image. **e** Otsu. **f** Improved Otsu

description of the main processing method. It should be noted that some of these methods can be classified into more than one category whose boundaries are not always unambiguous.

2.2.1 Line detection

As the laser stripe pattern geometrically made up of lines, methods are proposed that involve the detection of the lines directly from the input image. The combined equations of the detected lines represent the position of the laser stripe pattern and, therefore, the seam location. Methods that adopt integral transform algorithms such as the Radon transform [66] and Hough transform [67] to detect the laser lines in the image fall into this category [44, 56, 59]. In these methods, the image is first transformed into an integral or parametric space and points are selected to represent the detected lines in the original image, based on certain criteria. The researchers [44, 56] used a triangular-shaped laser stripe pattern whose lines are extracted using the Radon transform. The Radon transform is the projection of the image intensity along a radial line oriented at a specific angle. The input image is binarised first and labelled before applying the radon transform. With the Radon algorithm, a two-dimensional map of all the lines that can pass through a certain pixel of the original image is drawn. Each line is represented on the Radon map, according to its distance from the original image centre and its orientation (Fig. 7d). Therefore, the lines that are passing through more pixels have higher illumination values on the Radon map. By applying a local maxima algorithm on the Radon map, the line position and orientation in the real image can be detected. The complete image processing steps for the extraction of laser stripe

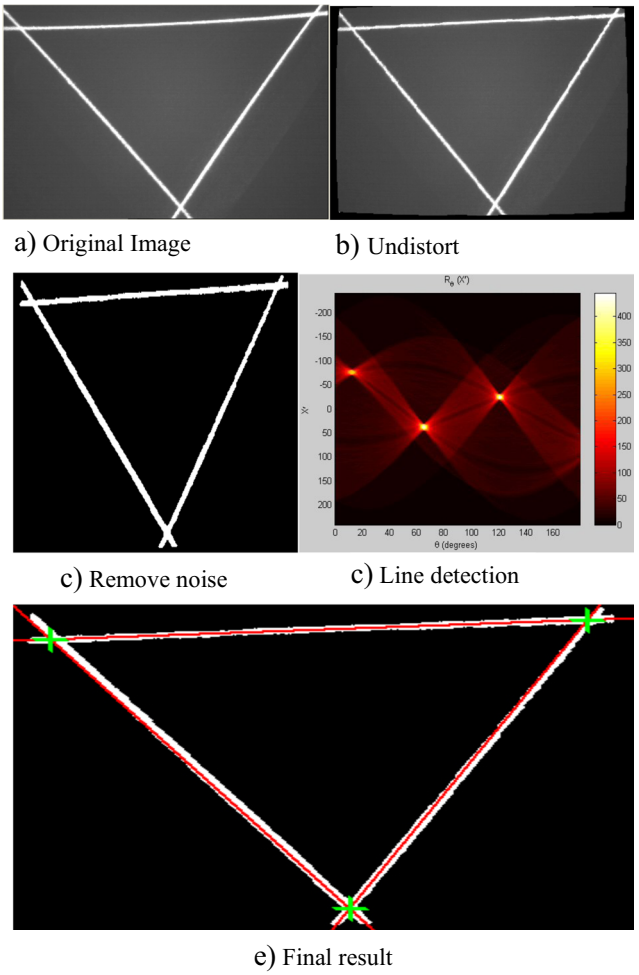

Fig. 7 Radon transform laser stripe line detection [44]. **a** Original image. **b** undistort. **c** Remove noise. **c** Line detection. **e** Final result

lines stated in [44, 56] are shown in Fig. 7. In [59], the Radon transform is also used in detecting a structured laser pattern in an input image containing a vertically oriented laser stripe. The Radon transform is used along both the horizontal and vertical directions. The brightest point in the map gives the position of the lines in the laser stripe. Despite its success in detecting lines, the Radon transform is computationally expensive algorithm.

2.2.2 Pixel maximum intensity

Due to the high-intensity values (higher brightness) at the region of the laser stripe, many researchers utilise this characteristic while extracting the laser stripe region [51–53, 55, 61, 68]. The idea behind maximum intensity strategy is to consider every row or column separately as a 1-dimentional signal depending on the orientation of the laser stripe as either horizontal or vertical. For horizontal laser stripe, columns in the image are treated independently. The row position in each column that has the maximum intensity value is selected as a point in the laser stripe. Combining these points from all the columns together generates the position of the laser stripe profile in the image. For a vertically oriented laser stripe, rows are treated independently. In [51], instead of the traditional maximum intensity strategy of taking one pixel with peak intensity, multi-peak has been proposed on a vertically oriented laser stripe as shown in Fig. 8. In this method, all pixels in each row with intensity values greater than certain threshold are marked and combined to form the laser stripe that has a thickness of more than 1 pixel. Additional filtration is then performed on the points based on selection criteria. One criterion is based on the fact that a laser stripe is represented by a narrow peak while distortions are much larger. Another criterion considers that the spatter noise by the arc light only occurs in a limited number of rows while laser reaches over large parts of the image frame. By performing neighbourhood search with these criteria in mind, the unwanted points are filtered out and a 1-pixel width laser stripe is extracted. In another related studies, when multiple pixels with the same maximum intensity values were encountered, the selection of the middle pixel among the multiple pixels is proposed as the chosen laser stripe profile location by some researchers [52, 61]. Because noisy maximum intensity pixels caused by false imaging might be selected, the researchers in [53] propose discarding some selected maximum intensity pixels based on temporal and spatial continuity constraints and the stripe profile is obtained using linear interpolation and Gaussian filtering. Maximum intensity method is not always limited to extracting a single laser line in an image; the researchers in [55] extract five laser stripe lines using maximum intensity method as shown in Fig. 9a. In the figure, the line AA^{-} represents a selected column of which all the five laser lines pass through. The lines are extracted by sorting the intensity values sequentially in descending order in each column and then taking the first five values as the position of the five lines in the column. In Fig. 9b, the intensity distribution of the column AA^{-} is shown. The five maximum peaks in Fig. 9b represent the line position in the column AA^{-}. The performance of the pixel-based maximum intensity algorithms is critically depended on the noise level, and therefore, it is crucial to remove the noisy artefacts before applying the method.

2.2.3 Sub-pixel maximum intensity

Some active vision systems may require higher measurement accuracy; this is why some researchers propose extracting maximum or peak position in each column or row at a sub-pixel accuracy, instead of the traditional maximum intensity that considers the maximum intensity of a pixel [69–72]. The distribution of the laser stripe should, in theory, be Gaussian distribution. But, in practice, owing to the behaviour of the camera sensors, the highly noisy environment and, to imperfections in the laser stripe, the observed cross section of the stripe may not be Gaussian. Nevertheless, to accurately detect the peak, methods such as Gaussian approximation [69], *centre of mass* [69], *linear interpolation* [69], Blais and Rioux [73] detectors and *parabolic estimator* [69] are used. The distinction among these methods depends on the assumption of the intensity distribution of the laser stripe. *Gaussian approximation* and *centre of mass assumed* that the spread of intensity values across the stripe conform to a Gaussian distribution. Linear interpolation assumes that a simple, linear relationship defines the spread of intensity values across the stripe. Assuming a horizontal laser stripe orientation, the peak position can be calculated by taking the three maximum intensity values and applying Eq. (2) for Gaussian approximation and Eq. (3) for centre of mass to calculate the position of the peak.

$$\text{Gaussian approximation}: \; x_{\text{peak}} = x - \frac{1}{2}\left(\frac{\ln(c) - \ln(a)}{\ln(a) + \ln(c) - 2\ln b}\right) \tag{2}$$

$$\text{Centre of mass}: \; x_{\text{peak}} = x + \frac{c - a}{a + b + c} \tag{3}$$

where a, b and c are the values of the three maximum intensity values with b being the maximum value. x is the column position of intensity b (the maximum) for the laser stripe. x_{peak} is the column position of the peak of laser stripe in a particular row. It can be observed from (3) that the centre of mass is simply a weighted average of the three maximum intensities. A comparative analysis on the effectiveness and accuracy of these sub-pixel methods was performed, and the results showed that the methods display performance within the same range [69]. Similar studies suggest that Gaussian

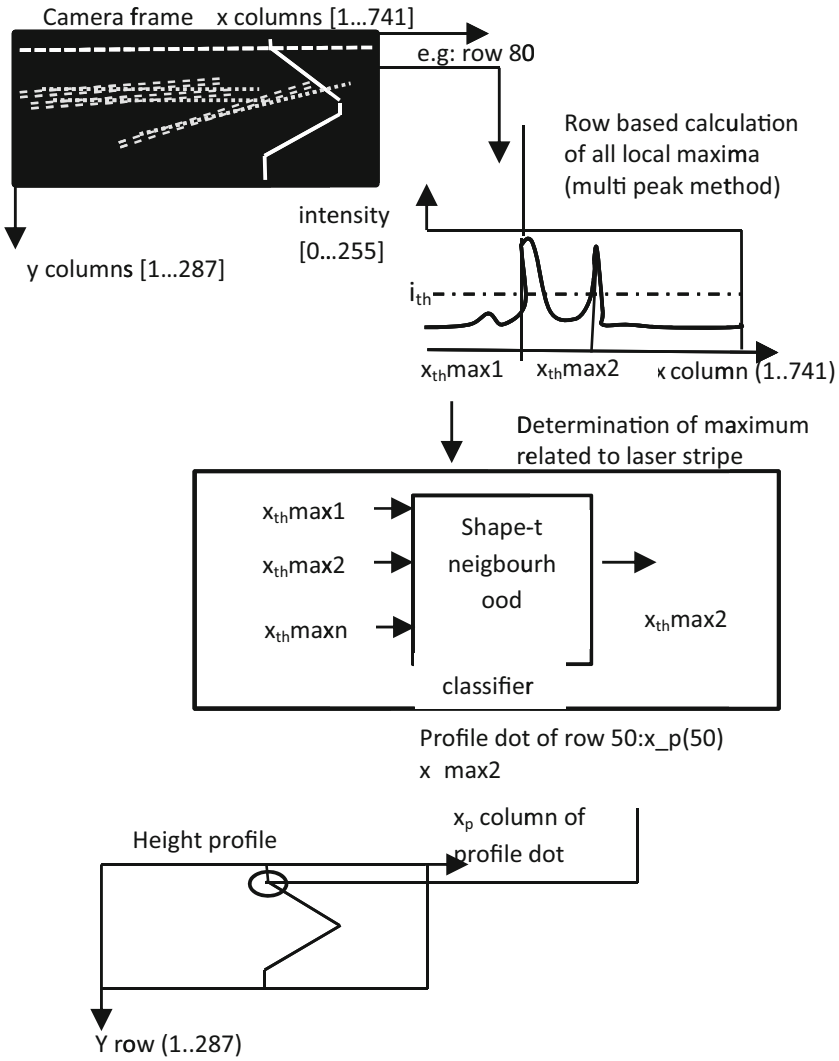

Fig. 8 Principle of multi-peak laser stripe detection algorithm [51]

approximation gives better performance especially when the noise level or stripe width decreases [74]. However, it was found that traditional maximum pixel intensity when combined with centre of mass gives the best accuracy [71]. In another study [70], the centre of mass method was employed to detect the peak at sub-pixel accuracy in a small window of size *W* around the maximum intensity using Eqs. (4) and (5) instead of using the three maximum intensities [69]. This method minimises the influences of reflection or surrounding light as claimed by the authors. Additionally, the detection process only holds if the difference between the light intensity of the maximum and the background is significant, i.e. higher

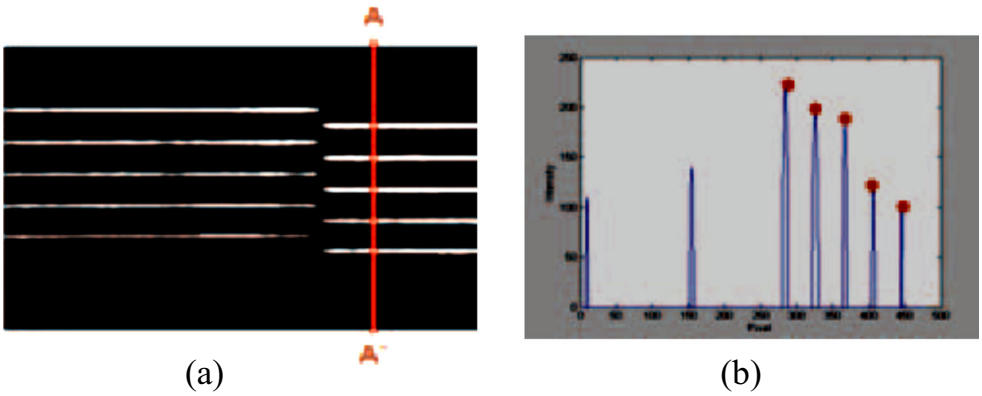

Fig. 9 **a** Column is selected by the line AA^{-}. **b** The intensity distribution of the column selected by the line AA^{-} [55]

than a threshold T. The background intensity is calculated by averaging the pixels outside the detection window which contains the maximum.

$$P_j = \begin{cases} CM_j(W) \ \ if \ \left(I\left[i^j_{\max},\ j\right] - B_j\right) > T \\ \text{none if } \left(I\left[i^j_{\max},\ j\right] - B_j\right) \le T \end{cases}. \tag{4}$$

$$CM_j(W) = \frac{\sum_{i^j_{\max}-\frac{W}{2}}^{i^j_{\max}+\frac{W}{2}} I[i,\ j]i}{\sum_{i^j_{\max}-\frac{W}{2}}^{i^j_{\max}+\frac{W}{2}} I[i,\ j]} \tag{5}$$

where P_j is the position for the laser stripe at column j and $CM_j(W)$ is the centre of mass of the window with a size W at column j. B_j is the good estimation of the background level for column j. $i^j_{\max}$ represents the row where the maximum light intensity is located for column j. Using this method, the laser stripe positions of some rows will be missing; as such, the authors propose a special method of filling missing positions considering contextual information around the missing points.

Further studies propose the computation of the zero crossing point of the first derivative of each laser stripe image row to obtain an estimation of the peak sub-pixel position [45, 75]. The first derivative of the input image is filtered first with finite impulse response (FIR) filter before the sub-pixel peak position is determined by the zero crossing point [76]. In another study [72], the authors consider the laser stripe width in implementing their proposed adaptive stripe peak segmentation algorithm with a sub-pixel precision. As with all other sub-pixel peak determination algorithms, the proposed algorithm treats each column in the image independently. For each column i, the laser stripe position is determined by first calculating its histogram h_i and extracting all peaks in the histogram greater than a threshold T_s which value determine for each column histogram h_i using the *algorithm* shown in Table 1. After thresholding, multiple peak groups can be found. A cost function defined by Eq. (6) is calculated for these peak groups. Then, the peak group whose cost is the smallest will be selected and the sub-pixel position will be extracted from the selected peak group using the centre of mass method [69].

$$cost_{\text{peak}} = \frac{|w_s - W_m|}{W_s} + \frac{|g_s - g_{\max}|}{g_{\max}} \tag{6}$$

where h_i denotes the histogram of the i^{th} column, W_μ denotes the standard stripe width, and W_σ denotes its tolerance. $C_{\min}$ denotes the minimum contrast between stripe and background, and $G_{\min}$ denotes the minimum reasonable grey. w_s and g_s are the peak group width and grey value, respectively.

2.2.4 Global thresholding

Some researchers propose the use of global thresholding on the input image to segment the laser stripe in the image [21, 43, 49, 60]. In [43], a threshold of 252 and a pixel following algorithm were proposed to denoise the thresholded image by taking into consideration the bandwidth of the laser in pixels. In another study, a global threshold of 90 was used to produce a binary image that distinctly separates the laser from the background [49]. The use of edge detection is proposed on the input image which is followed by the thresholding of the edge image in order to segment the laser stripe [50]. The authors in [4, 5] propose a thresholding based on intensity distribution of the pixels in the input image. The algorithm involves calculating the grey value of the image background by averaging the grey values of pixels along a logical grid lines spaced 10 pixels apart in both horizontal and vertical directions as described in (7).

Table 1 Stripe segment threshold determination

Algorithm 1: Stripe segment threshold determination
Input: h_i
Output: the existed T_s

1. Initialization: find the largest gray value g_{max} which makes the $h_i(g_{max}) \neq 0$; sum=0;
2. Threshold determination
   for k=g_{max} to 0
   If ($sum \geq W_\mu + W_\sigma$) OR ($g_{max} * k > C_{min}$), then stop loop
   End for
3. Post processing
   If($k > G_{min}$) then return $T_s = k$; else no T_s exists.

Source: [71]

$$B = \frac{1}{WM_1 + HM_2}\left(\sum_{i=1}^{W}\sum_{j=1}^{M_1} I(i,\ 10j) + \sum_{i=1}^{M_2}\sum_{j=1}^{H} I(10i, j)\right) \tag{7}$$

where W is the width of image and H is the height of image; $M_1 = Int(H/10)$; $M_2 = Int(W/10)$; $I(x, y)$ is the grey level of the image. Using a threshold T_1, the four points which define the laser stripe region ($Xmin$, $Xmax$, $Ymin$ and $Ymax$) are segmented using (8).

$$\begin{aligned} Xmax &= \max\{i : (I(i,\ 10j_1) - B > T_1) \vee (I(10i_1, j) - B > T_1)\} \\ Xmin &= \min\{i : (I(i,\ 10j_1) - B > T_1) \vee (I(10i_1, j) - B > T_1)\} \\ Ymax &= \max\{j : (I(i,\ 10j_1) - B > T_1) \vee (I(10i_1, j) - B > T_1)\} \\ Ymin &= \min\{j : (I(i,\ 10j_1) - B > T_1) \vee (I(10i_1, j) - B > T_1)\} \\ & 1 \le i \le W,\ 1 \le j \le H,\ i_1 = INT\left(\frac{i}{10}\right),\ j_1 = INT(j/10)\} \end{aligned} \tag{8}$$

In [77], windowing thresholding of the input image was performed to extract the laser stripe. A vertical 3-pixel window was used. The laser stripe is a horizontal oriented laser stripe. The window moves from top to bottom along five predetermined columns in the image, and the sum of the grey level of the window is compared with a threshold value. When the grey-level sum is greater than the threshold value, the point is set as an upper point of laser stripe at that column. Five sets of points obtained from the five columns define the upper part of the laser stripe. The lower part is obtained by moving the window from bottom to top. In [105], the threshold is determined based on the statistical distribution of the grey-level

values in the image to segment a horizontally oriented laser stripe. The grey level with the least number of pixels and closest to the highest grey value is chosen as the threshold. Single-point filtering is further performed to remove some of the noisy isolated points. The resulting laser stripe is further reduced to 1-pixel thickness by finding the edges in the image and taking the average of the edges in a column as the position of the laser stripe. Despite the reported implementations in the literature, the approaches based on the thresholding suffer from the fact that determination of the proper threshold value is not straightforward. These distinct characteristics of the thresholding prevent this approach from being commonly accepted practice in the segmentation of laser stripe in active vision systems.

2.2.5 Pixel projections

Laser stripe extraction by projection of the grey intensity or gradient values along the horizontal and vertical directions is another proposed technique [62, 63, 78]. In [62], region of interest (ROI) from the input image is first determined by thresholding the horizontal and vertical projections of the input image. Then, edge points corresponding to the boundary of the laser stripe are detected based on the criteria that the point with the largest gradient of grey value is the edge point in each row and column of the input image. Two edge points (upper edge point with the highest gradient value and lower edge point with the lowest gradient) were obtained along the vertical direction. Similarly, another two edge points (left edge point with highest gradient value and right edge point with lowest gradient value) were also obtained along the horizontal direction. The position of the laser stripe is then determined as the midpoints of the upper edge points and lower edge points in case of vertical while left and right edge points are determined in case of horizontal. In [78], unlike in [62], instead of projecting the intensity values, only the projection of the gradient values is performed. The upper edge points are then considered as the profile point of the laser stripe. Similarly, in [63], the projections are computed by skipping 1 pixel in both the horizontal and vertical directions in order to compute the ROI faster. An adaptive thresholding is then performed on the computed projections to determine the position of the laser stripe.

2.2.6 Statistical models

Most of the previously stated methods extract the laser stripe line from the perspective of filtering or noise suppression. However, the invariable illumination intensity along the laser stripe can be a good factor to consider in extracting the laser stripe. This is why some researchers formulate the image into sequence of states in space so that noisy states can be removed based on its transition at a particular point in space. The use of state-based statistical models such as spatial cascaded hidden Markov models (S-HMM) [79] to filter out noisy states and localise the region of the laser stripe in an image has been proposed by researchers [47, 80, 81]. The s-HMM was implemented after converting the input image into an edge image using Canny edge detector [82]. The edge pixels are then fed to the S-HMM as input observations or states as shown in Fig. 10. The output of the s-HMM gives the extracted laser stripe.

2.2.7 Second derivative filter

When the laser stripe is horizontally oriented, the stripe is believed to be parallel to the rows of the image. The laser stripe region in this context can be enhanced if convolved with a spatial filter that only operates in the direction of the image columns and yields a maximum response to the centre position of the stripe cross section. The Laplacian of Gaussian (LoG) filter [83] operates in this manner. In [84, 85], the input image is convolved with a discrete approximation of the second derivative Gaussian filter, given by (9) that depends on the thickness of the laser stripe and operates in the direction of the columns of the image. Because the laser stripe used by the authors is a horizontally oriented laser stripe, performing this technique can enhance the discrimination of the laser stripe from the other possible brightness sources such as arc glares and welding spatters. After applying (9) to the input image, the point along every column that corresponds to the maximum value among the filter responses in that column is extracted to form the position of the laser stripe in that column.

$$R(i,\ j) = \sum_{m=-3/2 L_w}^{3/2 L_w} w_m I(i,\ j+m) \tag{9}$$

where $I(i, j)$ denotes the pixel value at the image coordinates (i, j) and w_m is a filter coefficient that has a Mexican hat-like distribution. L_w is the estimated thickness of the laser stripe.

2.3 Welding joint feature extraction and profiling

The third step after the laser stripe profile extraction is the feature extraction. The feature extraction step involves the extraction of the relevant point from a laser stripe that identifies the deformed structural pattern on the welding joint. The feature points denote the turning points at the corners of the welding joint. The number and type of the turning points extracted depend on the welding joint configuration as shown in Fig. 11. The basic task in feature extraction is to identify these turning points. In an ideal condition, extracting these points could be a simple task of performing turning points/corner detection. However, in reality, the laser stripe extracted is far from its ideal shape. The straight lines are never straight, there might

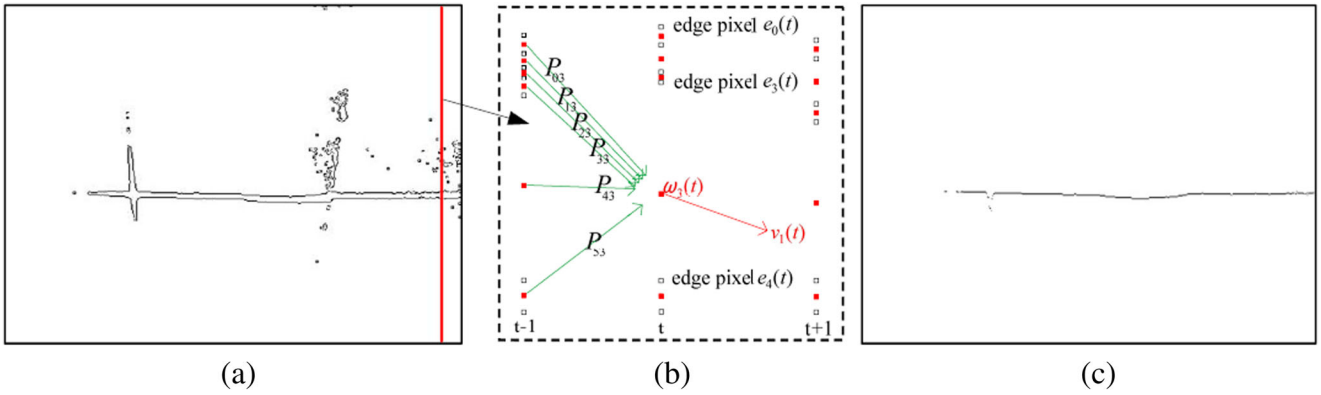

Fig. 10 Illustration of an s-HMM for stripe extraction. **a** Edge image and **b** illustration of the three steps of the s-HMM. The steps are from three columns of edge pixels of **a**, where *boxes* represent edge pixels and *square points* represent centre points of edge pairs, i.e. state ω of the s-HMM. P_{ij} is the transition probability from state i at step $(t–1)$ to state j at step t. **c** Extracted stripe skeleton [47]

be discontinuities along the lines, and noise could suppress these corners into higher or lower than their actual position. This makes it more challenging to actually detect these points. Researchers have proposed methods to efficiently detect these corners which will be reviewed in the following sub-sections.

2.3.1 Turning angle computation

The feature points are located along the laser stripe at the corners where the turning angle between these points and their neighbours is relatively large. This makes it possible to extract the points based on the characteristic nature of the turning angle [55, 57]. In [55], 'split and merge' [86] algorithm that filters out points based on their turning angles is used with template matching to extract the points. With the split and merge method, approximate straight line is generated from three points according to the turning angle between the points. Points in the stripe profile are scanned by considering three points at a time. A point is discarded as noise if the turning angle between the two lines joining the three points exceeds certain threshold as shown in Fig. 12. Tracking feature points are extracted by comparing the generated straight line with a welding joint pre-defined template. In [57], similar strategy of selecting the feature point based on the computed turning angle of a point is proposed. The feature points are determined by a set of rules based on the position and value of the turning angle at each point. The joint type used in the research is V-groove joint with three points (points 1, 2 and 3) as shown Fig. 11c. For each of the feature point, there exist associated rules that define the nature of the point as shown in Fig. 13. For example, the rules state that the position of the feature point 1 (x_0, y_0) must be on the right side of the starting point of the laser stripe; it is a turning point and its turning angle β must be less than 0 and greater than 90, and there is a right-side broken point below it within the range of 2 mm; the broken point should have a turning angle within [0, 90]; it is a left-side broken point, and its neighbouring point (x, y) should certify the criteria $x \geq x_0, y \geq y_0$. Similar rules hold for the remaining two points. The points that certify these respective criteria are selected as the feature points.

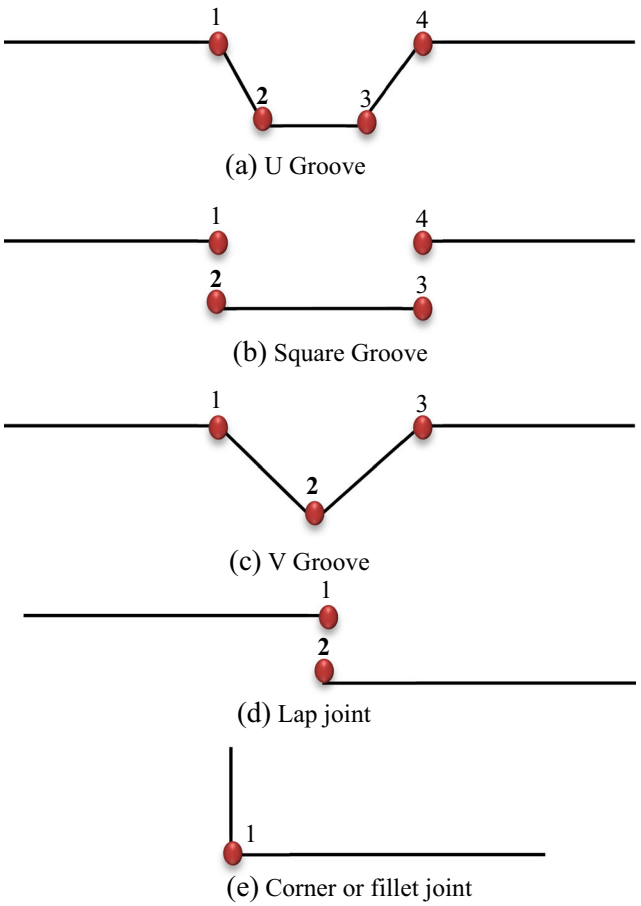

Fig. 11 Different welding joint feature points. **a** U groove. **b** Square groove. **c** V groove. **d** Lap joint. **e** Corner or fillet joint

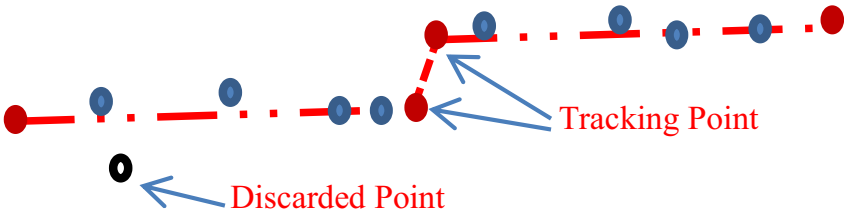

Fig. 12 Advance split and merge algorithm for the plane surface in a welded joint [55]

2.3.2 Image derivative

The extracted laser stripe can be treated as a one-dimensional signal with a discrete time steps. The feature points in the stripe can be considered as irregularities in the relative flow of the signal. Use of image derivatives [87] to detect these variations is prominent among researchers [3–5, 52, 53, 68, 77]. In [52], a method based on the second central difference (second CD) of the row index of each point in a horizontally oriented laser stripe profile is proposed. Second central difference is a discrete approximation of the first derivative. The second CD is computed for all the points in the laser stripe using (10). Based on the values of the second CD, a point scanning algorithm is proposed that searches for points that meet predefined criteria. The points obtained are selected and marked as the feature points.

$$CD\,(R_i) = \frac{R_{i+1} - R_{i-1}}{2} \tag{10}$$

where R_i is the row index of point i and R_{i+1} and R_{i-1} are the row indexes of the next and previous points in the laser stripe. In [77], a similar technique of adopting second CD to detect the feature points is proposed. The distinction comes from the computation of the CD itself. Instead of using (10) to compute the CD, (12) is used which is based on the accumulated grey-level intensity values in a column. Also, instead of the single-point search, a group of points that have CD value greater than 70 % of the maximum CD value is selected and the centre point in the group is selected as the position of the feature point.

$$CD(i) = \frac{I(i-k) + I(i+k) - 2I(i)}{2k} \tag{11}$$

where $I(i)$ is the grey-level sum of ith column in the laser stripe and $2k$ is the differential range for the CD. Experimentally, the authors established that a value of 6 is the appropriate value of the differential range irrespective of the weld joint gap. Instead of considering the variation in the relative positioning of the laser stripe points in detecting the feature points as in [52, 77], the intensity values of the stripe can be equally used [3–5, 53, 68]. The method involves computing the second derivative of the laser stripe, searching for the local minima and maxima of the derivative and selecting the points that correspond to the local maxima and minima as the feature points. In [3–5, 53], the Hough transform [67] is first employed to find a line that is approximately parallel to the laser stripe orientation and consider it as a reference line. The points from the laser stripe that are also located on the line are selected as the feature points in the welding workpiece plane. Extrema from the second derivative of the laser profile are then selected as the feature turning points. The process is depicted by Fig. 14.

2.3.3 Rule base

Most of the previously stated methods are applicable to only a specific joint geometry. However, researches have

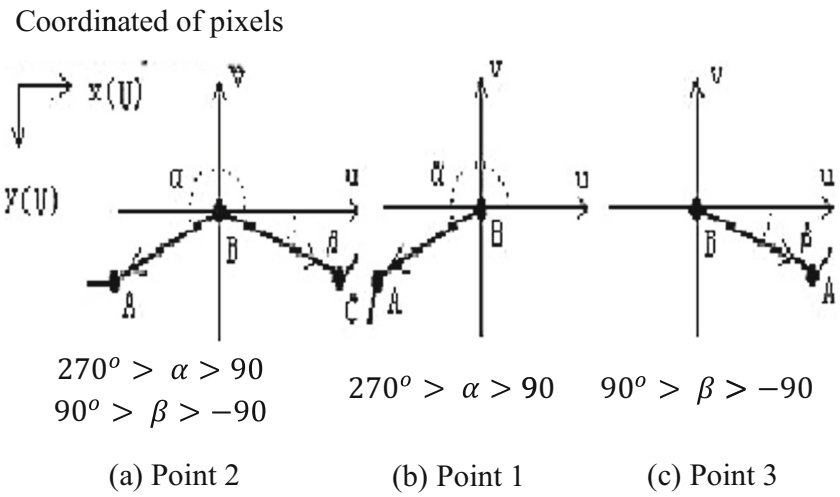

Fig. 13 Definition of feature points for V groove joint [57]. Points 1, 2 and 3 are defined in Fig. 11. **a** Point 2. **b** Point 1. **c** Point 3

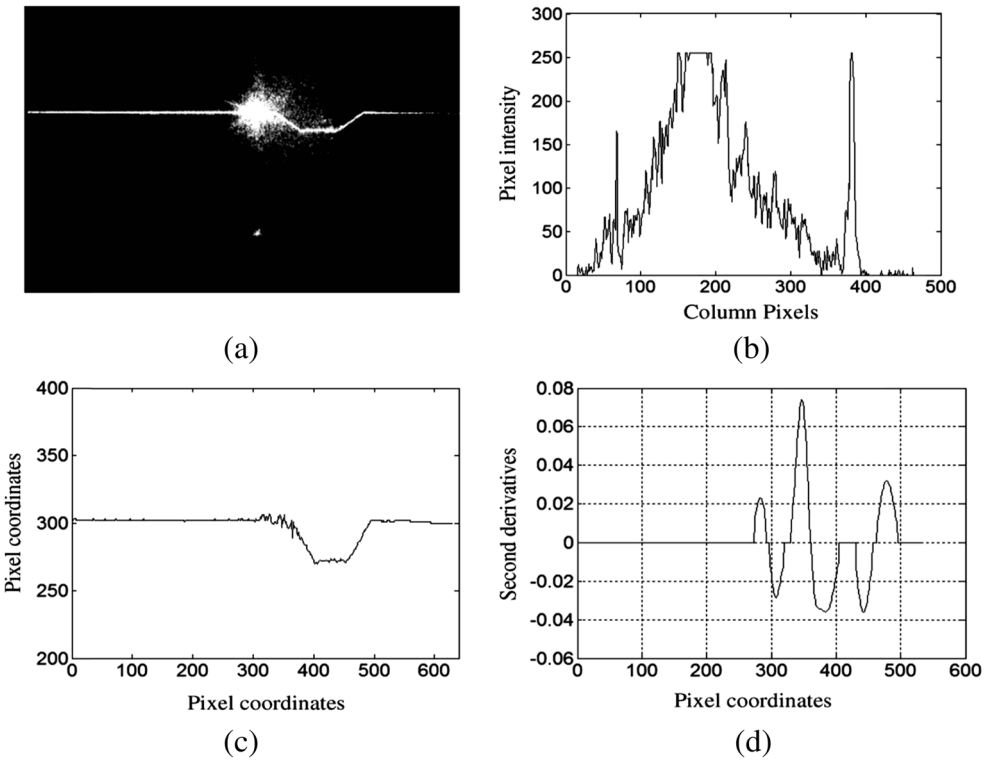

Fig. 14 Profile extraction of the laser stripes: **a** original image, **b** typical intensity distribution of column pixels, **c** extracted laser profile and **d** second derivative of the profile in **c** [53]

proposed rule-based approaches that can detect multiple joints geometry in one algorithm [71, 72, 84, 85, 88, 89]. The method involves approximation of the extracted laser profile into line segments. The line segments are labelled according to predefined welding segments. The labelled line segments are systematically combined to form a feature string. Based on certain defined criteria and classification methods, the feature string is interpreted to one of the known pre-defined welding joint type and the feature

Table 2 Line primitives and junction primitives

	Label	Description
Line Primitives	Speckle surface	
Junction Primitives	cp	
	cu	
	cd	
	gp	
	gu	
	gd	
	up	
	uu	
	ud	
	ap	
	au	
	ad	
	dp	
	du	
	dd	
	bp	
	bu	
	bd	

Source: [84]

Table 3 Generic models of typical joints

Type	Reference pattern language	profile
Fillet	<surface><cu><surface>	
Butt	<surface><gp><surface>	
	<surface><dp><surface><up><surface>	
	<surface><cd><surface><cu><surface><up><surface>	
	<surface><dp><surface><cu><surface><cd><surface>	
	<surface><cd><surface><cu><surface><cu><surface><cd><surface>	
Lap	<surface><cd><surface><cu><surface>	
	<surface><cu><surface><cd><surface>	
	<surface><dp><surface>	
	<surface><up><surface>	
Vee	<surface><cd><surface><cu><surface><cd><surface>	

Source: [84]

Table 4 Executive summary of techniques for active vision

Method	Comments and relative advantages
Image pre-processing	
Median filtering [21, 43, 48, 49, 55, 57–60]	This method is used by most researches, because it can keep the detail information such as edge pieces and sharp angles of seam. Also, it is the most effective in filtering typical welding image noise (predominantly salt-and-pepper noise).
Gaussian filtering [52, 58, 61]	Although among the most common and fundamental noise filters used in industrial applications, very few authors used this method. This is because it is not suitable for filtering laser images, as it can suppress the high-frequency component in the laser line image resulting in loss of useful positional information.
Multiple frame processing [3–5, 51, 53, 62, 63]	This method is mostly useful as an intermediary pre-processing step that can be followed by an additional filtering step. This is because it does not consider the spatial relationships of the local texture in the image that defines the laser pattern but rather considers the relative temporal texture information of multiple images.
Colour processing [47]	Although this method is ignored by most researches, this could be a potential pre-processing step to localise the laser pattern region in the image as it filters all colours except the characteristic red colour. However, this method may be somehow redundant when a narrow band optical filter is installed on the camera. This is because they are both useful in producing segmented red coloured image.
Thresholding [57, 58, 65]	This method may be effective when a suitable setup of optical devices is used that produces an image with an enhanced laser pattern. Such that, the laser pattern will have a relatively higher intensity that can be easily thresholded. However, optical devices are usually very expensive and very difficult to adjust to perfection.
Extraction of laser stripe pattern	
Line detection [44, 56, 59]	This method is useful in detecting 2D laser pattern with multiple lines in an image. It can be recommended for a fillet welding seam joint because the deformations of fillet joint usually are made of crossing lines as shown in Fig. 11e. However, this method is computationally expensive and can easily fail when the structural lines have multiple discontinuities. It can also falsely detect longitudinally shaped coherent noise due to arc light spatter in an image as a line.
Pixel maximum intensity [51–53, 55, 61, 68]	This is the most widely used laser stripe extraction method due to its simplicity and effectiveness. It is effective because it exploits the obvious characteristic of a laser stripe image which is high-intensity values (higher brightness). When combined with some custom pixel operations that employ pixel spatial and temporal relationships, it can produce a promising result.
Sub-pixel maximum intensity [69–72]	This is suitable for systems that need higher measurement accuracy. It provides an additional layer of processing and accuracy over the pixel maximum intensity method. However, with a very high-resolution cameras or wider welding seams, this method may give results that are almost similar to traditional pixel maximum intensity. This is because the laser pattern contains lesser position information.
Global thresholding [21, 43, 49, 60]	As with any thresholding technique, this method lacks universality and strongly depends on the quality and nature of the image under processing. In all the researches that fall in this category, the thresholding is performed with a value that is systematically computed. Although it was successful to some few researches, the distinct characteristics of the thresholding prevent this approach from being the commonly accepted practice in the segmentation of laser stripe in active vision systems.
Pixel projections [62, 63, 78]	This method is similar to pixel intensity approach as both detect pixels with higher brightness. The method could be more accurate due its additional edge detection step after the maximum pixel selection. However, the nature of the laser stripe uniform intensity distribution makes operations like edge detection unnecessary.
Statistical model [47, 80, 81]	With this method, the laser is extracted based on the notion that the laser can be modelled as series of states in space that can be analysed statistically. This method could be robust to noises that appear at an unusual location outside the laser region. However, it strongly relies on the state modelling step. As proposed by some of the authors, the states can be generated from the image pixel edges. Edge detection sometimes can produce broken edges which may lead to many false states that may affect the result of the final extracted laser.
Welding joint feature extraction and profiling pattern	
Turning angle computation [55, 57]	The turning angle is one of the unique characteristics that identify the feature points due to their strategic location along the laser stripe. Hence, this method can be effective in detecting the feature points. However, it is too localised, as it considers only two neighbours around a profile point. This algorithm performance can be affected when there are locally organised noisy points in the laser stripe. The performance may be improved if the turning angles for group of pixel neighbours are also considered.
Image derivative [3–5, 52, 53, 68, 77]	This method shows a more appealing approach of detecting the feature points. This is because the extracted profile is treated as one-dimensional signal that can be analysed with some 1-D signal processing techniques such as the image derivatives with the feature points treated as noise. This method presents the possibilities of using some other similar 1-D signal processing techniques that could be much more effective in detecting the feature points.
Rule base [71, 72, 84, 85, 88, 89].	This is one of the oldest and relatively robust approaches for the feature point extraction. It is effective because it employs prior knowledge in determining the location of the feature points. It also considers both the local and

Table 4 (continued)

Method	Comments and relative advantages
	global information of points before extracting the feature points. However, it is computationally expensive and strongly depends on the set of rules provided to it. The generation of the rules is also a challenging task as the rules are manually generated. It is not flexible to implement because any new noise challenge must be addressed by the rules. This method could be made flexible and much more effective when incorporated with some artificial intelligence algorithms such as artificial neural network and support vector machines that can automatically identify the rules.
Corner point detection [21, 58, 92]	This approach is closely similar to the turning point approach, as they both involve searching for the corner points. However, unlike in the turning point approach, the turning angle is not considered; rather general corner detection algorithms are used. This approach could be better than turning point because it does not involve primitive thresholding of turning angle to filter out points. However, as with the turning angle approach, this method is highly localised and can lead to noisy corners that may be due to the stripe profile orientation especially in wider laser stripe.
Custom pixel-to-pixel operation [43, 47, 59]	This method is too sensitive to noise due to the pixel-to-pixel operation. It also lacks universality as the pixel local distribution might vary across different laser stripe profiles. This method could be much more effective when incorporated with any of the other methods discussed previously.

points are extracted from the joint. In [84], the laser stripe profile is grouped into set of connected segments based on three-point connectivity. The connected segments are recursively approximated using polygonal line approximation method [90] into line segments. The generated line segments are refined and labelled by syntactic analysis of the segments. During the syntactic analysis, each line segment and junction between two neighbouring line segments are assigned a label in accordance with a predefined primitive vocabulary as shown in Table 2. The labelled segments form a feature string consisting of words. The string is further refined using some predefined production rules. Finally, the string that survives the revision process is matched to the pre-defined generic models of typical weld joints shown in Table 3. In [88], similar approach was adopted with less primitive vocabulary and production rules. Their analysis was based on using one-dimensional laser spot scanner image pattern [88] instead of the two-dimensional laser [84]. The authors in [84] claim that their algorithm has an improved performance over [88] from the viewpoint of robustness to noise and accuracy. In [71], after approximating the line segment for an extracted V-groove laser stripe profile, seven features are extracted from each segment which includes features such as length of segment, gradient and the distance to significant profile elements. These seven features are used as the inputs to a fuzzy algorithm [91] to calculate the degrees of membership for the right and left edges of the groove. The degree of membership and the coordinates of the line segments are then used to calculate the position of the left and right edges of the groove. Computing the mean value of left and right edges gives the groove position. The authors prove that their proposed fuzzy-based method is less dependent on segmentation parameters than the conventional rule-based algorithms.

2.3.4 Corner point detection

As stated previously, the feature points are strategically located at the corners along the laser profile as shown previously in Fig. 11. Hence, these points can be extracted by detecting corners in the extracted laser stripe. One notable approach for corner detection is by slope analysis [21, 58, 92]. From Fig. 11c, it can be observed that the V-groove has the left point (point 1), right point (point 2) and middle point (point 3). In [21, 92], only the left point and right point are considered relevant. The two points are extracted by slope analysis. Left corner point is extracted by calculating the slope at each point starting from the left most profile point. The left point is detected at the point where the slope exceeded certain threshold. Likewise, the right point is detected by starting from the right-most profile point. Slope at a point is obtained as the average slope of a few consecutive points around that point. The slope is calculated using (12).

$$k_{\text{slope}} = \frac{f(n) - f(n-k)}{k} \tag{12}$$

where $k = 1$ and $f(n)$ are the positions of the point n in the laser stripe profile. Another approach is by using the Harris corner detection algorithm [93] in detecting the corners [58]. However, the slope detection gives better performance than the Harris detector [58].

The corner point for a fillet welding joint configuration is the point of intersection of the two laser stripe lines as shown in Fig. 11e. The corner point in fillet weld can be detected by approximating the extracted laser stripe profile to line segments and finding the point of intersection of the two lines as the detected feature point [62, 63, 78]. In [62, 78], the feature lines are extracted by the combination of random sample consensus (RANSAC) [94] and least square line fitting algorithms [95]. RANSAC is applied to extract the two lines

followed by least square fitting of the two lines in order to improve the accuracy of the two lines. The intersection of the two extracted lines gives the feature point. In [63], a similar technique is adopted but with the Hough transform [67] which is employed first instead of RANSAC algorithm.

2.3.5 Custom pixel-to-pixel operation

Due to the non-flexibility of using conventional image processing operators, direct pixel-to-pixel search operation on the laser stripe profile has been adopted by researchers [43, 47, 59]. The operation involves scanning of the extracted profile point by point, evaluating each point based on its neighbours and selecting a point that meets certain criteria. In [59], an algorithm is proposed for extracting the feature points of a lap joint configuration shown in Fig. 11d. It involves searching from the leftmost point on the profile until the distance between the point and the next point is greater than a certain threshold; the point is marked as the first feature point (point 1 in Fig. 11d). Equally, the second feature point (point 2 in Fig. 11d) is found by searching from the rightmost point. In [47], the baseline of the laser stripe is first detected with the Hough transform. The search is performed with a window evaluated at each point in the extracted laser profile. The window is evaluated using (13).

$$M(w) = \frac{1}{|w|.\sigma^2}\left(s(w).\sum_{t\epsilon w}\left(P\left(\omega(t)\middle|\omega(t-1)\right)\right)\right)^{-1} \quad (13)$$

where w denotes current window with width $|w|$ and σ^2 is the variance of the values of the distance from points on the stripe to the baseline in the window. $s(w)$ is the number of pixels in the closed region between the convex line and the base. The larger the value of $M(w)$, the more likely the current window w contains the feature points. After the windowing operation on all the laser profile points, the local maximum points are detected as candidate feature point. The final feature points are detected from the candidate points by a temporal hidden Markov models (t-HMM) [79].

3 Discussion

In this paper, a review on the studies and contributions in the active vision methods has been presented. The aim was to highlight the challenges in the robotic welding and the methods proposed by the researchers to address these challenges. As there is no any avenue to fairly compare or evaluate the effectiveness of their proposed methods, this presentation only considers the methodology adopted or developed by different researchers. This is attributed to the fact that a fair comparison on the accuracy and performance of the available methods does not only depend on the image processing and pattern recognition algorithms, but also depend on other factors such as welding environment condition, image sensor type, camera resolution, calibration parameters, etc. In Table 1, although it is not exhaustive in terms of covering all methods, brief comments and the advantages of the commonly employed approaches are highlighted.

4 Conclusion

This paper has attempted to provide a comprehensive survey of research on vision-based intelligent robotic welding and also to offer some structural categories for the methods described in many papers. The major contribution of this paper has been to provide a brief source of reference for researchers involved in intelligent robotic welding. The difficulties and challenges due to the welding arc light and laser light reflection and scattering and the different image techniques to overcome these challenges have been discussed. A comparison between the different methods has been carried out where possible. However, because the images obtained in each study depend on the camera, laser and optics and system configuration, it was not possible in many cases to justify which method is more accurate or can provide accurate results. Despite these shortages, we have attempted to relatively compare these approaches based on their principle of implementation. Among many notable contributions in this subject, it is evident that there had been extensive research in the active vision and a more growing interest in passive vision can also be acknowledged. Collectively, the contributions discussed in this study have been summarised as in Table 4.

The scope of this study does not comprehensively cover the passive vision techniques, as such, future research could focus on the review of the passive vision approaches and contributions proposed by researchers.

Acknowledgments The authors would like to acknowledge the support provided by The Scientific and Technological Research Council of Turkey-TÜBİTAK (grant no. 114M756) for conducting this research work.

References

1. Pires JN, Loureiro A, Bölmsjo G (2006) Welding robots: technology, system issues and application. Springer Science & Business Media
2. Wilson WJ, Hulls CCW, Bell GS (1996) Relative end-effector control using Cartesian position based visual servoing. IEEE Trans Robot Autom 12(5):684–696
3. Xu D, Tan M, Zhao X, Tu Z (2004) Seam tracking and visual control for robotic arc welding based on structured light stereovision. Int J Autom Comput 1(1):63–75

4. Xu D, Wang L, Tan M (2004) Image processing and visual control method for arc welding robot. In: Robotics and biomimetics, 2004. ROBIO 2004. IEEE International Conference on (pp. 727–732). IEEE
5. Xu D, Jiang Z, Wang L, Tan M (2004) Features extraction for structured light image of welding seam with arc and splash disturbance. In: Control, Automation, Robotics and Vision Conference, 2004. ICARCV 2004 8th (Vol. 3, pp. 1559–1563). IEEE
6. Lanzetta M, Santochi M, Tantussi G (2001) On-line control of robotized Gas Metal Arc Welding. CIRP Ann Manuf Technol 50(1):13–16
7. Clarke T, Wang X (2000) The control of a robot end-effector using photogrammetry. Int Arch Photogramm Remote Sens 33(B5/1; PART 5), 137–142
8. Chen XZ, Huang YM, Chen SB (2012) Model analysis and experimental technique on computing accuracy of seam spatial position information based on stereo vision for welding robot. Ind Robot: Int J 39(4):349–356
9. Cook GE, Andersen K, Fernandez KR, Shepard ME, Wells Jr AM (1987) Electric arc sensing for robot positioning control. IFS(Publications) Ltd., Robotic Welding, 181–216
10. Park YW, Rhee S (2008) Process modeling and parameter optimization using neural network and genetic algorithms for aluminum laser welding automation. Int J Adv Manuf Technol 37(9–10): 1014–1021
11. Chaki S, Shanmugarajan B, Ghosal S, Padmanabham G (2015) Application of integrated soft computing techniques for optimisation of hybrid CO 2 laser–MIG welding process. Appl Soft Comput 30:365–374
12. Nele L, Sarno E, Keshari A (2013) Modeling of multiple characteristics of an arc weld joint. Int J Adv Manuf Technol 69(5–8): 1331–1341
13. Fridenfalk M (2003) Development of intelligent robot systems based on sensor control. Lund University
14. Fang Z, Xu D, Tan M (2013) Vision-based initial weld point positioning using the geometric relationship between two seams. Int J Adv Manuf Technol 66(9–12):1535–1543
15. Kiddee P, Fang Z, Tan M (2014) Visual recognition of the initial and end points of lap joint for welding robots. In: Information and Automation (ICIA), 2014 I.E. International Conference on (pp. 513-518). IEEE
16. Kong M, Shi FH, Chen SB, Lin T (2007) Recognition of the initial position of weld based on the corner detection for welding robot in global environment. In: Robotic welding. Springer, Berlin, pp 249–255
17. Zhu ZY, Lin T, Piao YJ, Chen SB (2005) Recognition of the initial position of weld based on the image pattern match technology for welding robot. Int J Adv Manuf Technol 26(7–8):784–788
18. Zhou L, Lin T, Chen SB (2006) Autonomous acquisition of seam coordinates for arc welding robot based on visual servoing. J Intell Robot Syst 47(3):239–255
19. Dinham M, Fang G (2013) Autonomous weld seam identification and localisation using eye-in-hand stereo vision for robotic arc welding. Robot Comput Integr Manuf 29(5):288–301
20. Micallef K, Fang G, Dinham M (2011) Automatic seam detection and path planning in robotic welding. In: Robotic welding, intelligence and automation. Springer, Berlin, pp 23–32
21. Li L, Fu L, Zhou X, Li X (2007) Image processing of seam tracking system using laser vision. In: Robotic welding, intelligence and automation. Springer, Berlin, pp 319–324
22. Chen XZ, Chen SB (2010) The autonomous detection and guiding of start welding position for arc welding robot. Ind Robot: Int J 37(1):70–78
23. Wei SC, Wang J, Lin T, Chen SB (2012) Application of image morphology in detecting and extracting the initial welding position. J Shanghai Jiaotong Univ (Sci) 17:323–326
24. Chen XZ, Chen SB, Lin T (2007) Recognition of macroscopic seam for complex robotic welding environment. In: Robotic welding, intelligence and automation. Springer, Berlin, pp 171–178
25. Dinham M, Fang G (2014) Detection of fillet weld joints using an adaptive line growing algorithm for robotic arc welding. Robot Comput Integr Manuf 30(3):229–243
26. Chen X, Chen S, Lin T, Lei Y (2006) Practical method to locate the initial weld position using visual technology. Int J Adv Manuf Technol 30(7-8):663–668
27. Nele L, Sarno E, Keshari A (2013) An image acquisition system for real-time seam tracking. Int J Adv Manuf Technol 69(9–12):2099–2110
28. Chen SB, Chen XZ, Qiu T, Li JQ (2005) Acquisition of weld seam dimensional position information for arc welding robot based on vision computing. J Intell Robot Syst 43(1):77–97
29. Shen HY, Wu J, Lin T, Chen SB (2008) Arc welding robot system with seam tracking and weld pool control based on passive vision. Int J Adv Manuf Technol 39(7–8):669–678
30. Xu Y, Fang G, Chen S, Zou JJ, Ye Z (2014) Real-time image processing for vision-based weld seam tracking in robotic GMAW. Int J Adv Manuf Technol 73(9–12):1413–1425
31. Gao X, Zhong X, You D, Katayama S (2013) Kalman filtering compensated by radial basis function neural network for seam tracking of laser welding. IEEE Trans Control Syst Technol 21(5):1916–1923
32. Baskoro AS, Masuda R, Kabutomori M, Suga Y (2009) An application of genetic algorithm for edge detection of molten pool in fixed pipe welding. Int J Adv Manuf Technol 45(11–12):1104–1112
33. Baskoro AS, Masuda R, Kabutomori M, Suga Y (2008) A comparison of particle swarm optimization and genetic algorithm for edge detection of molten pool in fixed pipe welding. In: SCIS & ISIS (Vol. 2008, No. 0, pp. 1743–1748). Japan Society for Fuzzy Theory and Intelligent Informatics
34. Baskoro AS, Kabutomori M, Suga Y (2009) Welding penetration control of fixed pipe in TIG welding using fuzzy inference system. J Solid Mech Mater Eng 3(1):38–48
35. Baskoro AS, Kabutomori M, Suga Y (2008) Automatic welding system of aluminium pipe by monitoring backside image of molten pool using vision sensor. J Solid Mech Mater Eng 2(5):582–592
36. Ge J, Zhu Z, He D, Chen L (2005) A vision-based algorithm for seam detection in a PAW process for large-diameter stainless steel pipes. Int J Adv Manuf Technol 26(9–10):1006–1011
37. Gao J, Wu C, Liu X, Xia D (2007) Vision-based weld seam tracking in gas metal arc welding. Front Mater Sci Chin 1(3):268–273
38. Gao XD, Na SJ (2005) Detection of weld position and seam tracking based on Kalman filtering of weld pool images. J Manuf Syst 24(1):1–12
39. Shen H, Lin T, Chen S, Li L (2010) Real-time seam tracking technology of welding robot with visual sensing. J Intell Robot Syst 59(3–4):283–298
40. Ohshima K, Morita M, Fujii K, Yamamoto M, Kubota T (1992) Sensing and digital control of weld pool in pulsed MIG welding. Trans Jpn Weld Soc 23(1):17–23
41. Bae KY, Lee TH, Ahn KC (2002) An optical sensing system for seam tracking and weld pool control in gas metal arc welding of steel pipe. J Mater Process Technol 120(1):458–465
42. Gao X, Ding D, Bai T, Katayama S (2011) Weld-pool image centroid algorithm for seam-tracking vision model in arc-welding process. IET Image Process 5(5):410–419
43. Gu WP, Xiong ZY, Wan W (2013) Autonomous seam acquisition and tracking system for multi-pass welding based on vision sensor. Int J Adv Manuf Technol 69(1–4):451–460
44. Iakovou D, Aarts R, Meijer J (2005) Sensor integration for robotic laser welding processes

45. Forest J, Salvi J, Cabruja E, Pous C. (2004) Laser stripe peak detector for 3D scanners. A FIR filter approach. In: Pattern Recognition, 2004. ICPR 2004. Proceedings of the 17th International Conference on (Vol. 3, pp. 646–649). IEEE
46. Xu P, Xu G, Tang X, Yao S (2008) A visual seam tracking system for robotic arc welding. Int J Adv Manuf Technol 37(1–2):70–75
47. Zhang L, Ye Q, Yang W, Jiao J (2014) Weld line detection and tracking via spatial-temporal cascaded hidden Markov models and cross structured light. IEEE Trans Instrum Meas 63(4):742–753
48. Xiao Z (2011) Research on a trilines laser vision sensor for seam tracking in welding. In: Robotic welding, intelligence and automation. Springer, Berlin, pp 139–144
49. Villán AF, Acevedo RG, Alvarez EA, López AC, García DF, Fernández RU, … & Sánchez JMG (2011) Low-cost system for weld tracking based on artificial vision. IEEE Trans Ind Appl 47(3): 1159–1167
50. Caggiano A, Nele L, Sarno E, Teti R (2014) 3D digital reconfiguration of an automated welding system for a railway manufacturing application. Procedia CIRP 25:39–45
51. Hang K, Pritschow G (1999) Reducing distortions caused by the welding arc in a laser stripe sensor system for automated seam tracking. In: Industrial Electronics, 1999. ISIE'99. Proceedings of the IEEE International Symposium on (Vol. 2, pp. 919–924). IEEE
52. Huang W, Kovacevic R (2012) Development of a real-time laser-based machine vision system to monitor and control welding processes. Int J Adv Manuf Technol 63(1–4):235–248
53. Li Y, Li YF, Wang QL, Xu D, Tan M (2010) Measurement and defect detection of the weld bead based on online vision inspection. IEEE Trans Instrum Meas 59(7):1841–1849
54. Kim JK, Hong JI, Kim JW, Choi DJ, Rhee SY (2012) Geometrical measurement about welding shape using dual laser vision system. In: Control, Automation and Systems (ICCAS), 2012 12th International Conference on (pp. 195–198). IEEE
55. Sung K, Lee H, Choi YS, Rhee S (2009) Development of a multi-line laser vision sensor for joint tracking in welding. Weld J
56. Iakovou D (2009) Sensor development and integration for robotized laser welding. University of Twente (Ph.D Thesis)
57. Shi YH, Wang GR, Li GJ (2007) Adaptive robotic welding system using laser vision sensing for underwater engineering. In: Control and Automation, 2007. ICCA 2007. IEEE International Conference on (pp. 1213–1218). IEEE
58. Lee JP, Wu QQ, Park MH, Park CK, Kim IS (2014) A study on optimal algorithms to find joint tracking in GMA welding. Int J Eng Sci Innov Technol 3:370–380
59. Zhang L, Wu C, Zou Y (2009) An on-line visual seam tracking sensor system during laser beam welding. In: Information Technology and Computer Science, 2009. ITCS 2009. International Conference on (Vol. 2, pp. 361–364). IEEE
60. Villán AF, Acevedo RG, Alvarez EA, López AC, García DF, Fernández RU, … & Sánchez JMG (2011) Low-cost system for weld tracking based on artificial vision. IEEE Trans Ind Appl 47(3), 1159–1167
61. Huang W, Kovacevic R (2011) A laser-based vision system for weld quality inspection. Sensors 11(1):506–521
62. Fang Z, Xu D (2009) Image-based visual seam tracking system for fillet joint. In: Robotics and Biomimetics (ROBIO), 2009 I.E. International Conference on (pp. 1230–1235). IEEE
63. Fang Z, Xu D, Tan M (2010) Visual seam tracking system for butt weld of thin plate. Int J Adv Manuf Technol 49(5–8):519–526
64. Piccardi M (2004) Background subtraction techniques: a review. In: Systems, man and cybernetics, 2004 I.E. international conference on (Vol. 4, pp. 3099–3104). IEEE
65. Otsu N (1975) A threshold selection method from gray-level histograms. Automatica 11(285–296):23–27
66. Toft PA, Sørensen JA (1996) The Radon transform-theory and implementation (Doctoral dissertation, Technical University of Denmark Danmarks Tekniske Universitet, Department of Informatics and Mathematical Modeling, Institut for Informatik og Matematisk Modellering)
67. Ballard DH (1981) Generalizing the Hough transform to detect arbitrary shapes. Pattern Recogn 13(2):111–122
68. Li Y, Wang QL, Li YF, Xu D, Tan M (2008) On-line visual measurement and inspection of weld bead using structured light. In: Instrumentation and Measurement Technology Conference Proceedings, 2008. IMTC 2008. IEEE (pp. 2038–2043). IEEE
69. Naidu DK, Fisher RB (1991) A comparative analysis of algorithms for determining the peak position of a stripe to sub-pixel accuracy. In: BMVC91, 1991st edn. Springer, London, pp 217–225
70. Usamentiaga R, Molleda J, García DF (2012) Fast and robust laser stripe extraction for 3D reconstruction in industrial environments. Mach Vis Appl 23(1):179–196
71. Haug K, Pritschow G (1998) Robust laser-stripe sensor for automated weld-seam-tracking in the shipbuilding industry. In: Industrial Electronics Society, 1998. IECON'98. Proceedings of the 24th Annual Conference of the IEEE (Vol. 2, pp. 1236–1241). IEEE
72. Gong Y, Dai X, Li X (2010). Structured-light based joint recognition using bottom-up and top-down combined visual processing. In: Image Analysis and Signal Processing (IASP), 2010 International Conference on (pp. 507–512). IEEE
73. Blais F, Rioux M (1986) Real-time numerical peak detector. Signal Process 11(2):145–155
74. Trucco E, Fisher RB, Fitzgibbon AW, Naidu DK (1998) Calibration, data consistency and model acquisition with laser stripers. Int J Comput Integr Manuf 11(4):293–310
75. Forest Collado J (2004) New methods for triangulation-based shape acquisition using laser scanners. Universitat de Girona
76. Khoury JM (1999) U.S. Patent No. 5,931,898. U.S. Patent and Trademark Office, Washington, DC
77. Kim JW, Bae HS (2005) A study on a vision sensor system for tracking the I-butt weld joints. J Mech Sci Technol 19(10):1856–1863
78. Fang Z, Xu D, Tan M (2011) A vision-based self-tuning fuzzy controller for fillet weld seam tracking. IEEE/ASME Trans Mechatron 16(3):540–550
79. Eddy SR (1996) Hidden Markov models. Curr Opin Struct Biol 6(3):361–365
80. Zhang L, Jiao J, Ye Q, Han Z, Yang W (2012) Robust weld line detection with cross structured light and Hidden Markov Model. In: Mechatronics and Automation (ICMA), 2012 International Conference on (pp. 1411–1416). IEEE
81. Zhang L, Ke W, Han Z, Jiao J (2013) A cross structured light sensor for weld line detection on wall-climbing robot. In: Mechatronics and Automation (ICMA), 2013 I.E. International Conference on (pp. 1179–1184). IEEE
82. Canny J (1986) A computational approach to edge detection. IEEE Trans Pattern Anal Mach Intell 6:679–698
83. Marr D, Hildreth E (1980) Theory of edge detection. Proc R Soc Lond B Biol Sci 207(1167):187–217
84. Kim JS, Son YT, Cho HS, Koh KI (1996) A robust visual seam tracking system for robotic arc welding. Mechatronics 6(2):141–163
85. Kim JS, Son YT, Cho HS, Koh KI (1995) A robust method for vision-based seam tracking in robotic arc welding. In: Intelligent Control, 1995. Proceedings of the 1995 I.E. International Symposium on (pp. 363–368). IEEE
86. Xiao Y, Zou JJ, Yan H (2001) An adaptive split-and-merge method for binary image contour data compression. Pattern Recogn Lett 22(3):299–307
87. Aubert G, Kornprobst P (2006) Mathematical problems in image processing: partial differential equations and the calculus of variations (Vol. 147). Springer Science & Business Media

88. Sicard P, Levine MD (1989) Joint recognition and tracking for robotic arc welding. IEEE Trans Syst Man Cybern 19(4):714–728
89. Nan H, Beattie RJ, Davey PG (1988) A rule-based system for interpreting weld seam images. Int J Adv Manuf Technol 3(3): 111–121
90. Pavlidis T, Horowitz SL (1974) Segmentation of plane curves. IEEE Trans Comput 8:860–870
91. Berkan RC, Trubatch S (1997) Fuzzy system design principles. Wiley-IEEE Press
92. Wu J, Smith JS, Lucas J (1996) Weld bead placement system for multipass welding. IEE Proc: Sci Meas Technol 143(2):85–90
93. Harris C, Stephens M (1988) A combined corner and edge detector. In: Alvey vision conference (Vol. 15, p. 50)
94. Fischler MA, Bolles RC (1981) Random sample consensus: a paradigm for model fitting with applications to image analysis and automated cartography. Commun ACM 24(6):381–395
95. York D (1968) Least squares fitting of a straight line with correlated errors. Earth Planet Sci Lett 5:320–324